



Highly efficient removal of organic dyes and heavy metal cation from wastewater by polyphenolate porous coordination polymer

H. Y. Ye¹ · H. Xu¹ · C. Z. Wu¹ · B. Li¹ · J. Z. Guo¹

Received: 5 August 2022 / Revised: 30 December 2022 / Accepted: 18 February 2023 / Published online: 9 March 2023

© The Author(s) under exclusive licence to Iranian Society of Environmentalists (IRSEN) and Science and Research Branch, Islamic Azad University 2023

Abstract

Seeking efficient, reusable, and low-budget adsorbent materials for the removal of industrial effluent is of great interest for the community of environmental chemistry. In this work, a mesoporous phenolic resin-type polymer was successfully synthesized by one-step solvothermal synthesis starting from two relatively cheap polymer monomers (i.e., phloroglucinol and 4,4'-Biphenyldicarboxaldehyde), and it exhibited excellent adsorption capacity toward both methylene blue (728.63 mg/g) and Pb (II) (176.08 mg/g) at 308 K. Based on a variety of characterizations on this material and a systematic study on the effect of various working conditions (including concentration, temperature, pH value, and ionic strength), we conclude that the adsorption for methylene blue and Pb(II) on phenolic resin-type polymer was consistent with pseudo-second-order kinetic equation ($R^2 > 0.98$) and Langmuir model ($R^2 > 0.97$); adsorptions were thermodynamically endothermic and occurred spontaneously; adsorptions were driven by the electrostatic interaction between phenolic resin-type polymer and Methylene blue or Pb (II). Our research demonstrated the potential application of phenolic resin-type polymer in the elimination of two different types of pollutants from wastewater.

Keywords Adsorption · Methylene blue · Pb (II) · Phenolic resin-type polymer

Introduction

Heavy metal cations and organic dyes are common pollutants in wastewater from industry, and such waste must be carefully treated before being released to the environment. Among the many techniques developed for wastewater-treatment, the one based on an adsorption-separation process is still the most popular due to its high efficiency and easy operation. So far, many materials such as zeolite, activated carbon and resin have been selected as adsorbents (Chairunnisa et al. 2020; Lian et al. 2020; Liu et al. 2020; Mansha et al. 2020; Salehi et al. 2020; Muscarella et al. 2021), but their relatively low adsorption capacity and poor reusability limit their application. Developing more efficient and

reusable adsorbent materials is thus of great significance (Jayasanth Kumari et al. 2017).

Porous organic polymers (POPs) that characterized by large exposing surface, high porosity, controllable geometric structures, and tunable functionalities are promising adsorbents. POPs are usually synthesized by polymerization of various organic monomers, which can endow them with abundant structures and binding / catalytic sites, making them potential in gas adsorption, chemical sensing, separation, and catalysis (Lu et al. 2021). Moreover, their molecular structures that constructed by strong covalent bonds show excellent chemical stability, allowing them to work in harsh environment (like wastewater with different pH values or redox properties). As a typical POP, porous phenolic resin-type polymer (PRP) can be obtained easily by the polymerization of 4,4'-Biphenyldicarboxaldehyde with phloroglucinol (which is an important chemical intermediate for pharmaceutical synthesis, dye coupling agent, tire tackifier, azo composite ink and other raw materials) through the C–C coupling (Huang et al. 2009; Kim and Kim 2010). It is well-known that the ortho and para carbon atoms in a phenyl ring structure are rich of electrons (donated by the hydroxy group), while the carbonyl group in an aldehyde molecule

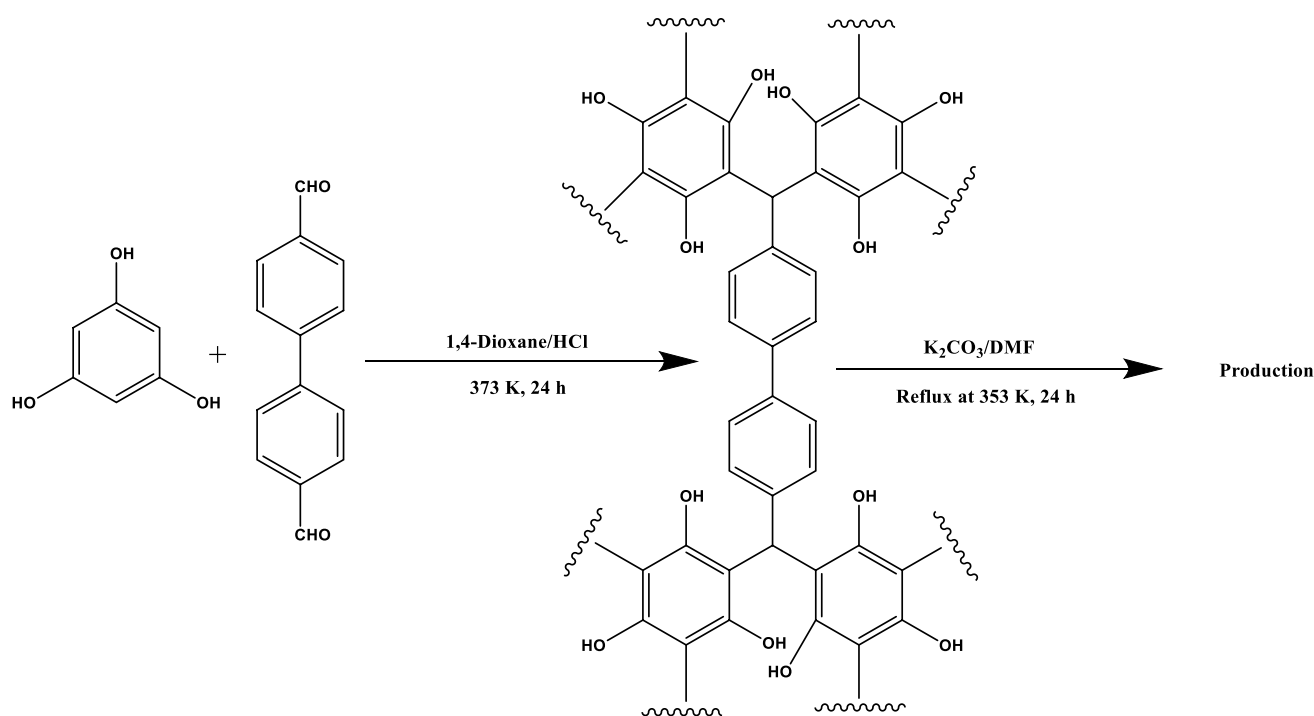
Editorial responsibility: Chenxi Li.

H. Y. Ye and H. Xu have contributed equally to this paper.

✉ J. Z. Guo
guojianzhong@zafu.edu.cn

¹ College of Chemistry and Materials Engineering, Zhejiang A & F University, Hangzhou 311300, Zhejiang, People's Republic of China





Scheme 1 The synthetic approach of PRP adsorbent

lacks electron (i.e., positively charged). Thereby, a nucleophilic substitution reaction can easily occur between them: one carbonyl group bonds with two phenols by eliminating one water molecule, resulting in a cross-linked polymer with abundant hydroxyl groups.

In the current work, a porous phenolic resin-type polymer was specifically designed for the elimination of heavy metal cations (e.g., Pb (II)) and organic dyes (e.g., methylene blue) in wastewater. This material was prepared by a simple one-step solvothermal synthesis using two relatively cheap and common polymer monomers (i.e., phloroglucinol and 4,4'-Biphenyldicarboxaldehyde) as precursors at a lower temperature in the presence of hydrochloric acid. Then, the influence of reaction conditions (such as the pH value, the concentration of adsorbates and the solvent ionic strength) was systematically studied and the working mechanism was discussed. Our work demonstrated the potential of PRP as an outstanding adsorbent toward both cationic dyes and heavy metal cations in wastewater.

Materials and methods

Chemicals

Phloroglucinol, 4,4'-Biphenyldicarboxaldehyde, hydrochloric acid, 1,4-Dioxane, N,N-dimethylformamide

(DMF), tetrahydrofuran (THF), potassium carbonate (K₂CO₃), methylene blue (MB, C₁₆H₁₈N₃ClS), lead nitrate (Pb(NO₃)₂) were all purchased from Shanghai Aladdin Biochemical Technology Co., Ltd. (Shanghai, China) and used directly and there is no additional refinement.

Preparation of adsorbent

The porous phenolic resin-type polymer was synthesized through a one-pot solvothermal method as described in Scheme 1. Typically, 5 g of phloroglucinol and 3.15 g of 4,4'-Biphenyldicarboxaldehyde were dissolved in 200 ml of 1,4-Dioxane at a Teflon lined autoclave. Then, the above admixture was first agitated at ambient temperature for 5 min, then hydrochloric acid (20 mL) was added. After mixing, the system was heated to 373 K and kept for 24 h. The intermediate product was filtrated, rinsed with THF, ethyl alcohol, and distilled water in a row after cooling to room temperature, and finally dried in an oven at 60 °C.

3 g of the intermediate product and 2.1 g of potassium carbonate were added to the flask containing 500 mL of DMF. Then, then it was heated to 353 K and kept refluxed about 24 h. The precipitate was rinsed sufficient by distilled water after cooling to room temperature, and then dispersed to a solution of NaOH (0.1 mol/L) for another treatment of 3 h. The final product was obtained by washing and

filtering using distilled water, and then dried at 60 °C for 24 h (product labeled as PRP adsorbent).

Characterization

Fourier transform infrared (FT-IR) spectrums were recorded with Nicolet, Magna 550 spectrometer. The transmission tests of each sample were obtained using KBr as diluent. The nitrogen adsorption–desorption isotherms were recorded on an Autosorb-iQ2 automated gas-sorption analyzer (Quantachrome Instruments, USA). Thermogravimetric (TG) analysis was carried out by using Shimadzu TGA-50 thermal analyzer. Basically, each sample (10 mg) was heated from ambient temperature to 800 °C at a ramp of 5 °C/min in N₂ ambience. Zeta potentials were tested on the Zetasizer Nano-ZS (Malvern Instruments). Scanning electron microscopy (SEM) and the related energy-dispersive X-ray spectroscopy (EDS) were analyzed on a Zeiss Supras 55 equipped with EDX detector.

Adsorption property

The adsorption property of PRP under different conditions was evaluated by controlling the initial pH values, contact time, inceptive MB or Pb (II) concentration, the dose of adsorbent, temperature, etc. For a typical test, 40 mg PRP was dispersed in 50 mL solution with MB or Pb (II) in a 150 mL Erlenmeyer flask. It was horizontally vibrated at a rate of 110 rpm in trembling incubator. An aliquot of the solution was collected after shaking for a certain time, and a clear solution was obtained after filtration by membrane filter (pore size was 0.45 μm). The elimination of Pb (II) was tested by AA-6880F atomic absorption spectrometer (Shimadzu) while that of MB was determined by UV 759S spectrometer at λ_{max} = 664 nm after a proper dilution of both solutions.

The removal efficiency and adsorption capacity of PRP adsorbent were estimated using the forthcoming Eqs. (1) and (2):

$$R(\%) = \frac{(C_o - C_e)}{C_o} \times 100 \quad (1)$$

$$q_e = \frac{(C_o - C_e)V}{W} \quad (2)$$

where R (%) represents the portion of Pb (II) or MB that has been removed, C_o (mg/L) is the fresh concentration, while C_e is the adsorption equilibrium concentration. V (L) is the solution volume. W (g) is the PRP adsorbent weight.

Adsorption model

Adsorption isotherm

The adsorption isotherms were then fitted by Langmuir (Eq. (3)) (Langmuir 1916) model and Freundlich (Eq. (4)) (Freundlich 1906) model as shown as follows:

$$q_e = \frac{Q_o K_L C_e}{1 + K_L C_e} \quad (3)$$

$$q_e = K_F C_e^{1/n} \quad (4)$$

where C_e (mg/L) is equilibrium concentration of contaminant in a solution, while q_e (mg/g) represents equilibrium adsorption capacity of pollutant on PRP. Q_o (mg/g) is the maximum adsorption capacity that achieved by PRP. K_L (L/mg) is the Langmuir adsorption constant. The bigger K_L , the stronger the adsorption capacity of the adsorbent. K_F (mg^{1-1/n}·L^{1/n} g⁻¹) is the Freundlich affinity constant. $1/n$ was the adsorption heterogeneity factor. The smaller $1/n$, the stronger the adsorption capacity of the adsorbent.

Adsorption kinetics

To further understand the kinetics of the adsorptions, the experiment data were fitted by different models, including the pseudo-first-order (Eq. 5) and pseudo-second-order (Eq. 6) models (Ho and McKay 1999; Li et al. 2020a) as shown as follows:

$$q_t = q_e (1 - e^{-k_1 t}) \quad (5)$$

$$q_t = \frac{q_e^2 k_2 t}{1 + q_e k_2 t} \quad (6)$$

where q_e (mg/g) represents equilibrium adsorption capacity, while q_t (mg/g) stands for the adsorption capacities as the time change. k_1 (min⁻¹) and k_2 (g·mg⁻¹·min⁻¹) represent the first- and second-order rate constants, respectively.



Adsorption thermodynamics

Thermodynamic calculations were carried out to explore the influence of temperature on the adsorption performance. Basically, enthalpy change (ΔH° , $\text{kJ}\cdot\text{mol}^{-1}$) and the standard entropy change (ΔS° , $\text{J}(\text{mol}\cdot\text{K}^{-1})$) were obtained from the slope and the intercept of Van't Hoff equation (Eq. 7). The standard free energy change (ΔG° , $\text{kJ}\cdot\text{mol}^{-1}$) was worked out based on the isothermal equation (Eq. 8) (Qian et al. 2018; Lima et al. 2019).

$$\ln K_e^\circ = \frac{\Delta S^\circ}{R} - \frac{\Delta H^\circ}{RT} \quad (7)$$

$$\Delta G^\circ = -RT \ln K_e^\circ \quad (8)$$

$$K_e^\circ = \frac{1000\Delta K_L\Delta C_o\Delta M}{\gamma}$$

where K_e° is the thermodynamic equilibrium constant, K_L represents Langmuir adsorption constant, $T(K)$ is the Kelvin temperature, and R is molar gas constant, γ is the coefficient of activity, C_o is the standard concentration of the adsorbate ($1\text{ mol}\cdot\text{L}^{-1}$), M is the molecular weight of adsorbate.

Reusability of adsorbent

For the reusability of the PRP, 40 mg of PRP was placed into 50 mL of $100\text{ mg}\cdot\text{L}^{-1}$ Pb (II) solution at pH 5. The Pb (II)-loaded PRP was separated by filtration and reproduced by sinking in 50 mL of $0.1\text{ mol}\cdot\text{L}^{-1}$ HCl solution for 6 h, and then the adsorbent was filtered and washed with deionized water. Then, the adsorbent was activated by immersing in $0.1\text{ mol}\cdot\text{L}^{-1}$ NaOH for 2 h before the next cycle of adsorption.

Results and discussion

Characterization of PRP

Various techniques were adopted to characterize the as-synthesized PRP or the one after adsorption test.

FTIR analysis

Figure 1c, d and e illustrates the FTIR spectra of as-synthesized PRP and the ones after adsorption of MB and

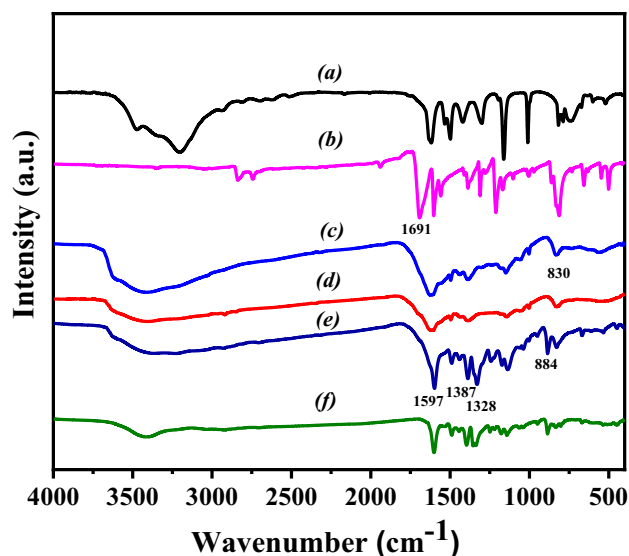


Fig. 1 FT-infrared spectrum **a** Phloroglucinol, **b** 4,4'-Biphenyldicarboxaldehyde, **c** PRP, **d** After adsorption on PRP for Pb^{2+} , **e** After adsorption on PRP for MB and **f** MB

Pb (II). A strong band appeared in all the three samples at 3430 cm^{-1} that was assigned to the stretching mode of $-\text{OH}$ (Peng et al. 2017; Sun et al. 2021), coming from phloroglucinol (Fig. 1a). The PRP with enriched hydroxyl groups might be advantageous for Pb(II) adsorption by complexation with O-containing groups. From Fig. 1a and b, the typical band at 1691 cm^{-1} is assigned to the adsorption of $\text{C}=\text{O}$ from 4,4'-Biphenyldicarboxaldehyde (Wu et al. 2014). However, this band disappeared in PRP (Fig. 1c and d), indicating that the $\text{C}=\text{O}$ functional group was destroyed during the condensation reaction. The peak of 830 cm^{-1} belonged to the disubstituted benzene ring. Characteristic peaks of the MB molecule were detected in the PRP adsorbent after adsorption of MB (Fig. 1f): the band at 1597 cm^{-1} might be attributed to $\text{C}=\text{N}$ vibration; peak at 1387 cm^{-1} was due to the symmetric stretching of $\text{C}-\text{N}$; the band of 1328 cm^{-1} was ascribed to the symmetric deformation of methyl (Lv et al. 2022). Noteworthy, vibration peaks of aromatic ring of MB shifted from 826 to 884 cm^{-1} and from 1589 to 1597 cm^{-1} after adsorbing onto PRP (Li et al. 2019), while another two peaks that initially located at 1319 cm^{-1} and 1389 cm^{-1} were moved to 1328 and 1387 cm^{-1} , respectively, indicating a strong interaction between the phenolic hydroxyl of PRP and the methyl group (i.e., $-\text{N}(\text{CH}_3)_2^+$) of MB. Furthermore, the existence of abundant aromatic rings in the adsorbent can result in the occurrence of $\pi-\pi$ interactions between

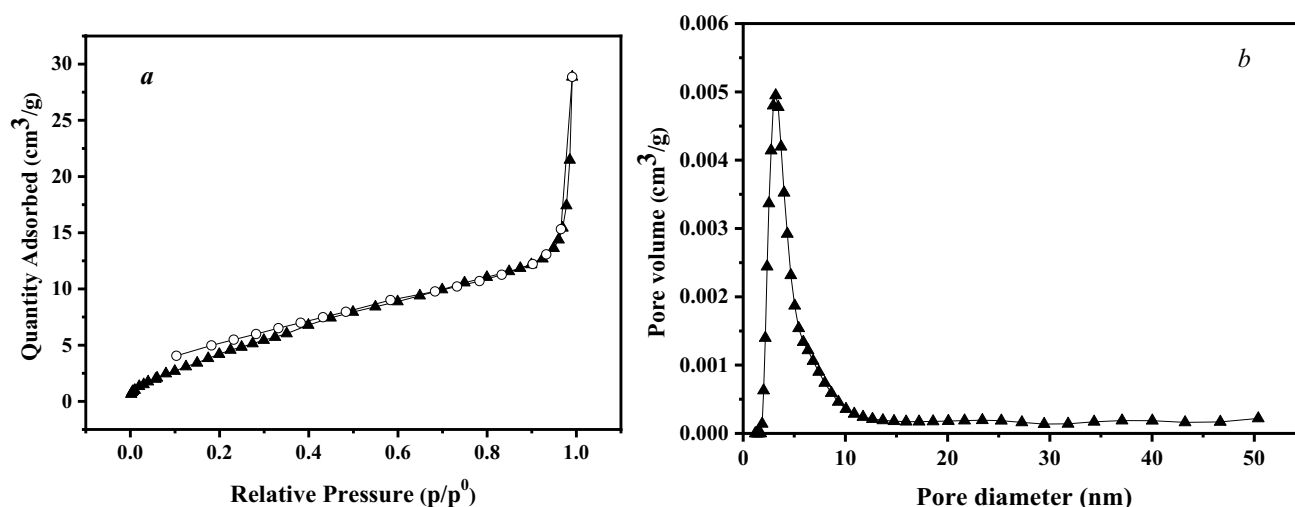


Fig. 2 **a** N_2 adsorption–desorption isotherms and **b** pore size distribution of mesoporous PRP adsorbent

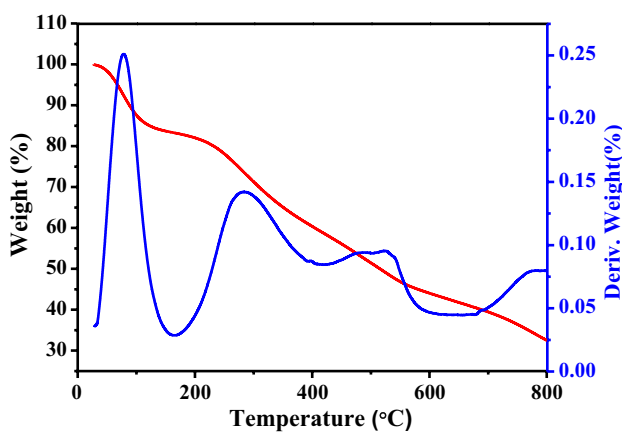


Fig. 3 The TGA curve of PRP in air atmosphere

hollow PRP and MB molecules during the adsorption process (Fu et al. 2015).

N_2 adsorption surface analysis

The N_2 adsorption–desorption analysis on PRP shows a type IV isotherm. It indicates the prevalence of mesoporous structure in PRP (Fig. 2a) with the pore size distributed at 2–10 nm (Fig. 2b) and on average at 8.4 nm. The BET specific surface area of PRP was $21.19 \text{ m}^2/\text{g}$ by calculation, while the pore volume was $0.0447 \text{ cm}^3/\text{g}$.

TGA analysis

Figure 3 gives thermal behavior of PRP that was analyzed based on TGA analysis. Basically, the sample underwent three different steps of weight decline and with a total loss of up to 70.0% from room temperature to 800 °C. The first step that occurred at $\sim 100 \text{ }^\circ\text{C}$ (approximately 16.81%) might be

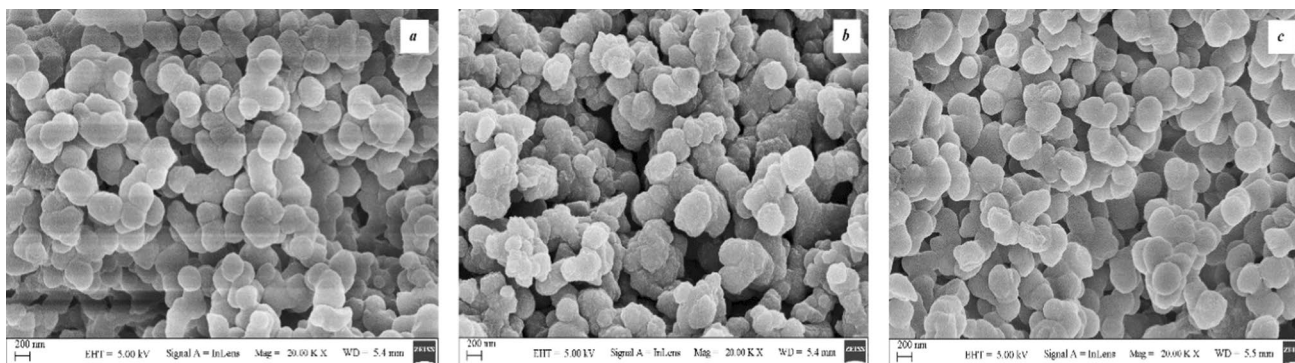
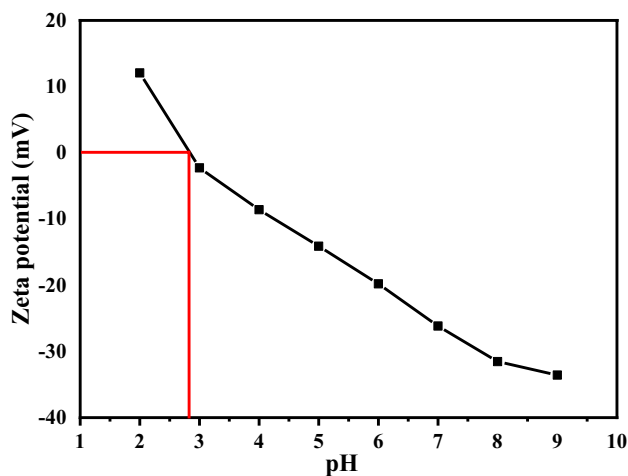


Fig. 4 morphology of **a** the as-synthesized PRP, **b** the PRP after adsorption of MB, and **c** the PRP after adsorption of Pb(II)



Table 1 EDS elements of PRP, PRP-MB and PRP-Pb (II)

Element							
Content wt%	C	O	Na	S	Cl	Pb	Total
PRP	71.95	27.96	0.09	–	–	–	100
PRP-MB	72.32	21.7	0.06	5.87	0.05	–	100
PRP-Pb (II)	60.74	16.23	0.07	–	–	22.96	100

**Fig. 5** The surface Zeta potentials of PRP at different pH values

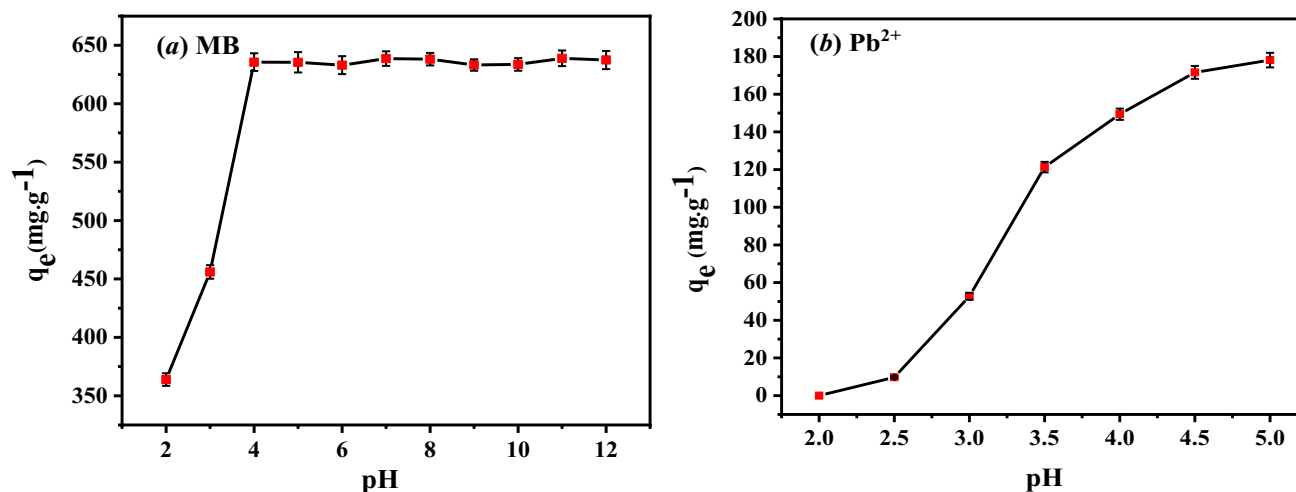
caused by the evaporation or desorption of adsorbed water, while the second weight loss (about 51.35%) that occurred at 300 °C ~ 500 °C might be due to the decomposition of the polymer backbone chain (Vinodha et al. 2020).

SEM–EDS analysis

Figure 4 gives the SEM results of PRP both before and after the adsorption of pollutants. The as-prepared PRP appeared as uniform microspheres with smooth surface (Fig. 4a). However, the N₂ adsorption–desorption results suggest that they might be stacked by smaller particles, forming internal mesoporous channels. After capturing pollutants, the surface of PRP became slightly rougher (Fig. 4b and c), and the adsorbed MB or Pb (II) on their surface could be confirmed by EDS as shown in Table 1. EDS shows the surface of PRP contains C, O, Na elements. After MB and Pb(II) adsorption, the contents of C, S, Cl and Pb increase, respectively, while Na and O contents decrease, which also verifies that MB was adsorbed on the surface of PRP and that ion exchange mechanism between Na⁺ and MB occurred during adsorption.

Zeta potential analysis

Figure 5 shows the correlation between the zeta potentials of PRP and pH of the solution. When pH soared from 2.0 to 9.0, zeta potentials gradually decreased from +12.1 mV to –33.6 mV. The PRP exhibited a point of zero charge

**Fig. 6** Adsorption capacity of PRP toward **a** MB and **b** Pb (II) at different pH values

(pH_{ZPC}) of about 2.8. At a pH value higher than it, the PRP became negatively charged so that can efficiently adsorb heavy metal cations and cationic dyes through the electrostatic interaction.

Influence of pH value

Figure 6 shows the adsorption of MB and Pb (II) on PRP at different pH values. The adsorption of MB was discussed at a pH range of 2.0–12.0. From Fig. 6a, it turned out that the uptake capacity of the PRP adsorbent for MB enhanced evidently from 363.87 mg/g to 635.48 mg/g when pH increased from 2.0 to 4.0. Further increase in the pH value did not change the adsorption anymore, indicating that the adsorption of MB on PRP reached a saturation. This correlation between adsorption capacity and pH was consistent with the literature (Li et al. 2021). On the other hand, the adsorption of Pb (II) cations was only evaluated at a pH range of 2.0–5.0 due to the formation of lead hydroxide in neutral or alkaline environment. It shows that the super low adsorption capacity of Pb (II) at pH of 2.5 (only 9.76 mg·g⁻¹) was sharply increased to 178.14 mg·g⁻¹ (pH = 5.0) (Fig. 6b).

At low pH values, the protonation of PRP would suppress the adsorption of MB or Pb²⁺ on its surface. However, the deprotonation of hydroxy occurs on PRP with the increasing of pH, resulting in a negative charge of PRP surface, which might be favor for the adsorption of positively charged MB and Pb (II). Meanwhile, hydrogen bonding occurs easily between N atoms on the phenothiazine in MB and C–OH of PRP. All the above results indicated that pH value could significantly affect the electrostatic interaction between the pollutants and PRP adsorbent, thereby that enhance the elimination efficiency of pollutants from wastewater (Zheng et al. 2018).

Adsorption isotherms

The adsorption isotherms that show the equilibrium amount of MB or Pb (II) adsorbed on the surface of PRP in different solutions (i.e., with different concentrations) and at different temperatures (e.g., 298, 303 and 308 K) were displayed in Fig. 7. Evidently, higher temperatures favor the adsorption, suggesting an endothermic nature of this process. From Fig. 7 and Table 2, which give the fitting results, Langmuir isotherm exhibits a higher R^2

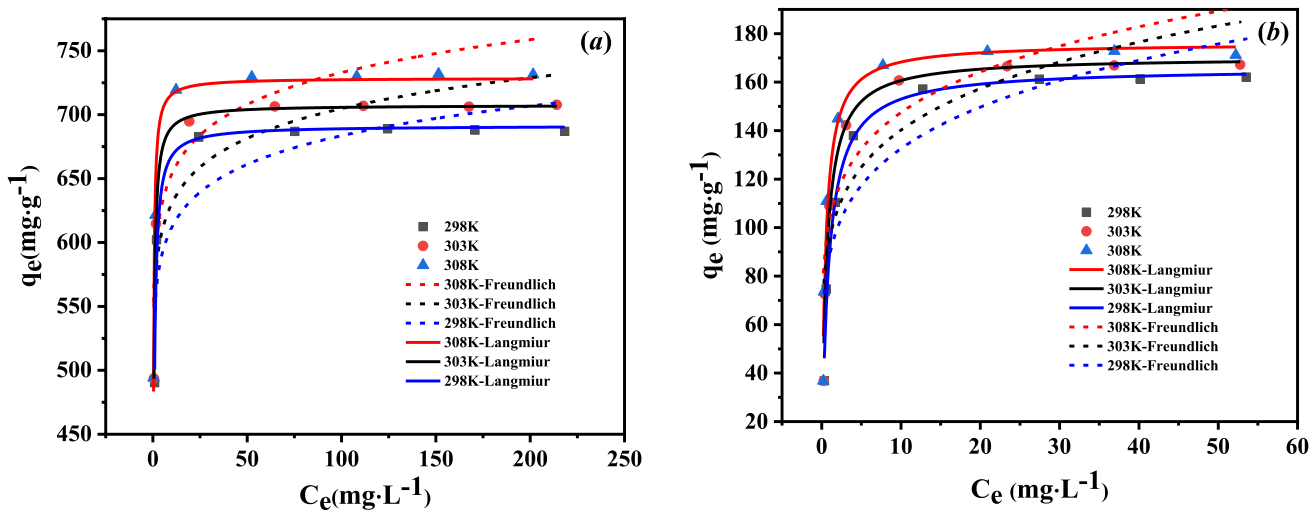


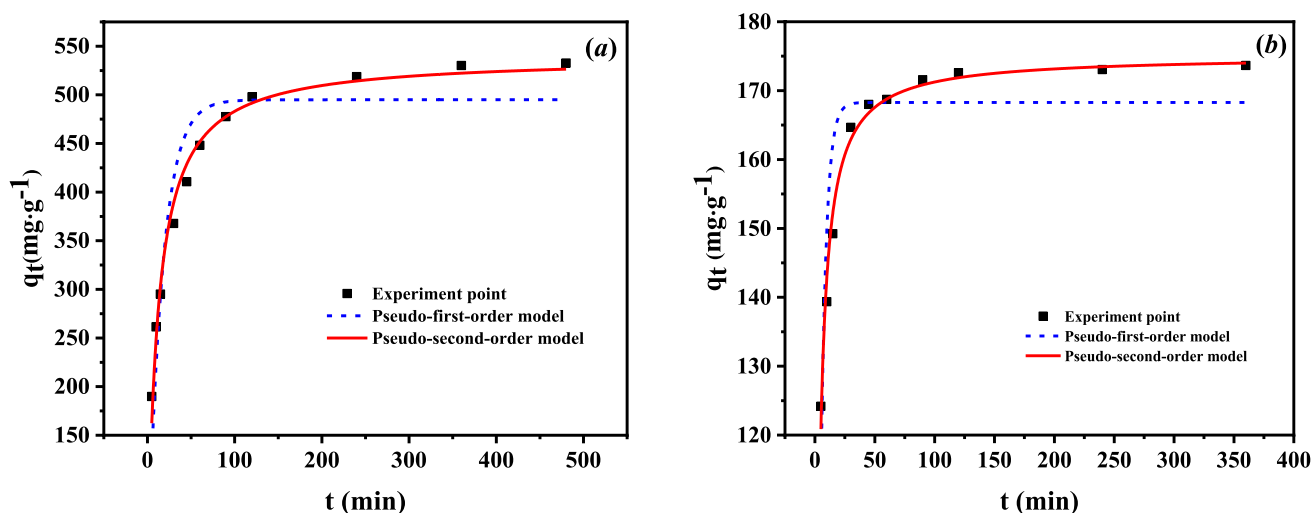
Fig. 7 The Langmuir and Freundlich fittings of the MB a and Pb (II) b adsorption isotherms at different temperatures

Table 2 The optimized parameters for Langmuir and Freundlich models

Adsorbate	T (K)	q _e (exp)	Langmuir equation			Freundlich equation		
			Q ₀ (mg·g ⁻¹)	K _L	R ²	K _F	1/n	R ²
MB	298	687.01	691.41	2.8080	0.9860	547.37	0.04528	0.7496
	303	707.66	707.51	3.9304	0.9995	563.77	0.04847	0.7741
	308	731.43	728.63	5.5477	0.9820	582.57	0.04985	0.7757
Pb (II)	298	162.10	165.87	1.1887	0.9880	88.56	0.1752	0.7937
	303	167.25	170.33	1.6627	0.9758	95.63	0.1662	0.7743
	308	171.19	176.08	2.1604	0.9705	103.19	0.1551	0.7367

Table 3 Comparison of MB/Pb (II) adsorption by various adsorbents

Adsorbate	Adsorbents	q_e (mg/g)	References
MB	Triptycene based-hydroxyl-azo-polymer	250	Ansari et al. (2020)
	Bifunctional anionic metal-organic Framework	149	Zhou et al. (2018)
	TPT-DMBD-COF	45.45	Huo et al. (2019)
	Oxone-treated hydrochar	33.79	Madduri et al. (2020)
	ZnCl ₂ -modified Bamboo hydrochar	47.3	Li et al. (2020b)
	PRP	728.63	This work
Pb (II)	H ₂ O ₂ -modified hydrochar of peanut hull	22.82	Xia et al. (2019)
	H ₂ O ₂ -modified hydrochar of pinewood sawdust	92.8	Xue et al. (2012)
	Dithiocarbamate-functionalized porous lignin	200	Li et al. (2015)
	Alkali-modified hydrochar of grape pomace	137	Petrović et al. (2016)
	Dithiocarbamate group-functionalized graphene oxide	132.10	Gao et al. (2017)
	Amine/imine (-NH ₂ /-NH) and dithiocarbamate (-CSS-)	79.9	Wang et al. (2019)
	PRP	176.08	This work

**Fig. 8** The kinetic fittings of the MB **a** and Pb (II) adsorption curves**Table 4** The optimized parameters for the pseudo-first-order and pseudo-second-order fittings

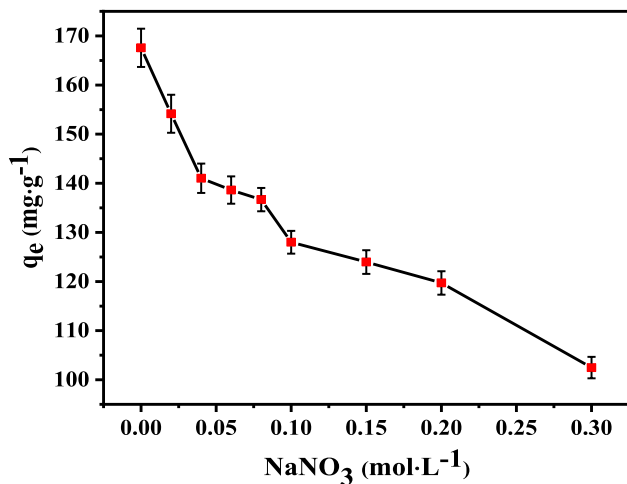
Adsorbate	T (K)	$q_{e(\text{exp})}$ (mg·g ⁻¹)	Pseudo-first-order			Pseudo-second-order		
			q_e (mg·g ⁻¹)	K_1 (min ⁻¹)	R^2	q_e (mg·g ⁻¹)	k_2 (mg·g ⁻¹ ·min ⁻¹)	R^2
MB	303	532.66	494.95	0.0601	0.8856	539.13	1.6×10^{-4}	0.9850
Pb (II)	303	173.64	168.28	0.02221	0.7844	175.09	2.55×10^{-3}	0.9830

($R^2 = 0.9705\text{--}0.9995$) value and its q_e was closer to the Q_0 . This indicated a higher quality of the fitting with Langmuir model, rather than Freundlich model, and the adsorption process was monolayer adsorption. The Langmuir equation is suitable for homogeneous adsorption systems where the

adsorption of each adsorbate molecule has equal activation energy. Maximum adsorption of 728.63 mg/g for MB and 176.08 mg/g for Pb (II) were achieved by PRP at 308 K, which were much larger than most adsorbents reported previously (Table 3).

Table 5 The thermodynamic fitting results for the MB and Pb (II) adsorptions

Adsorbate	T(K)	$\Delta G(\text{kJ}\cdot\text{mol}^{-1})$	$\Delta H(\text{kJ}\cdot\text{mol}^{-1})$	$\Delta S(\text{J}\cdot\text{mol}^{-1}\cdot\text{K}^{-1})$	R^2
MB	298	-33.96	51.95	288.27	0.9997
	303	-35.38			
	308	-36.85			
Pb (II)	298	-30.76	45.62	256.40	0.9962
	303	-32.12			
	308	-32.32			

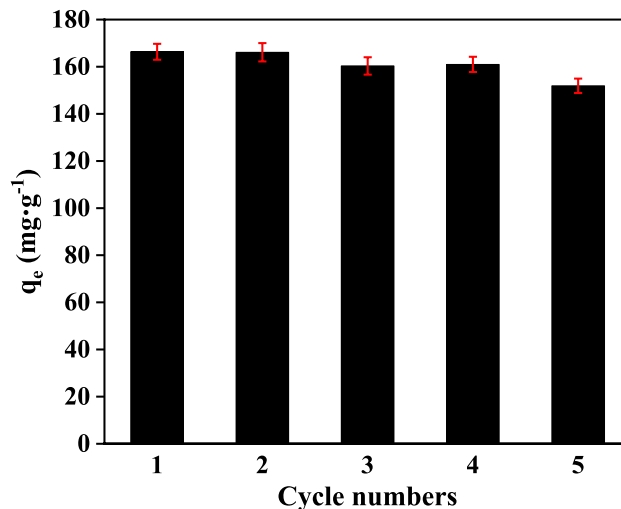
**Fig. 9** Ionic strength effects on the Pb (II) adsorption

Kinetic analysis

The adsorption curves of MB and Pb (II) ions in Fig. 8 show that the adsorption processes were fast within the first 30 min as more than half of Pb (II) and more than 95% of MB were removed from the solution. Noteworthy, the adsorption processes slowed down significantly as time extends, and they finally attained stable platform mainly due to a full coverage of their surface by the adsorbates. Our fitting results in Table 4 clearly manifest that pseudo-second-order model ($R^2 = 0.99, 0.98$, respectively, at 303 K) fitted our results very well. Thereby, both MB and Pb (II) cations follow the second-order kinetics.

Thermodynamic calculations

The thermodynamic results were given in Table 5. ΔH value indicates that the adsorption can be attributed to chemisorption (Pang et al. 2017). The positive ΔH and the negative ΔG values in Table 5 indicated that adsorption of pollutants onto PRP was endothermic process and could

**Fig. 10** Reusability of PRP as an adsorbent on Pb (II) adsorption

happen spontaneously at the working temperatures. These results could also explain why higher temperatures favor the adsorption process (as shown in Fig. 7). By increasing the temperature from 298 to 308 K, ΔG for MB adsorption decreased from -33.96 to -36.85 kJ/mol, while that for Pb (II) decreased from -30.76 to -32.32 kJ/mol. This indicated a stronger thermodynamic driving force for the adsorption at higher temperatures. Moreover, the positive ΔS° obtained indicated an enhanced randomness at higher temperatures, and this was conducive to an adsorption process.

Effect of ionic strength

In another check experiment, NaNO_3 was joined into Pb (II) solution to enhance its ionic strength. As the result given in Fig. 9, adsorption capacity of PRP from Pb (II) declined evidently from $167.57 \text{ mg}\cdot\text{g}^{-1}$ to $102.48 \text{ mg}\cdot\text{g}^{-1}$ with the dosage of NaNO_3 increase from zero to 0.3 mol/L. In principle, increasing the solvent ionic strength would reduce the



electrostatic potential between the adsorbents and adsorbates. Thereby, our control experiment claimed that electrostatic interaction might be one of essential role and adsorption mechanism in the adsorption of pollutants.

Regeneration experiments

To prove that PRP is a reusable adsorbent, we tested its reusability by investigating the adsorption and desorption of Pb (II) on PRP (Fig. 10). The Pb (II)-loaded PRP can be regenerated easily by immersing in HCl solution because PRP hardly absorbed Pb (II) in the range of $\text{pH} < 2$ (Fig. 6b). From Fig. 10, the adsorption capacity of Pb (II) onto PRP was maintained above 90% after 5 cycles. These results clearly demonstrated that PRP can be easily recycled with high adsorption ability.

Conclusion

Mesoporous PRP that enriched with hydroxyl groups was successfully synthesized by a one-step solvothermal synthesis from two relatively cheap polymer monomers. It exhibited excellent adsorption capacity toward both MB ($728.63 \text{ mg}\cdot\text{g}^{-1}$) and Pb (II) ($176.08 \text{ mg}\cdot\text{g}^{-1}$) at 308 K, and both adsorbent processes were consistent with the Langmuir and pseudo-second-order model. Experiments at various pH and ionic strength revealed that the attractive interaction between the pollutants (positive) and the PRP adsorbent (negative) dominated the adsorption process. The electrostatic interaction, hydrogen bonding, ion exchange and complexation might be the critical controlling mechanisms over MB and Pb (II) adsorption, while π - π interaction plays minor roles. Our work provides some basic principles for the design of cheap PRP adsorbent, which could be further extended to a wide range of pollutants in wastewater.

Acknowledgements This research had been supported by the National Natural Science Foundation of China under Grant Number 32271528 and U1932126; and the Zhejiang Province “Vanguard” and “Leading Goose” Research and Development Project under Grant Number 2022C02036.

Author contributions All authors contributed to the study’s conception and design. HYY and HX contributed equally to this paper. The experimental design, material preparation, and background research were performed by HYY, HX, BL, JZG; data collection and analysis were conducted by HYY, HX, CZW. The first draft of the manuscript was written by HYY, HX, and all authors commented on previous

versions of the manuscript. All authors have read and approved the final manuscript.

Funding National Natural Science Foundation of China, 32271528, Jianzhong Guo, 12175200, Bing Li; Zhejiang Province “Vanguard” and “Leading Goose” Research and Development Project, 2022C02036.

Data availability All data and materials used in this study can be provided by the corresponding author on reasonable request.

Declarations

Conflict of interest The authors declare that they have no conflict of interest.

Ethical approval This article does not contain any studies with human participants or animals performed by any of the authors.

Consent to participate Not applicable.

Consent to publish Not applicable.

References

- Ansari M, Alam A, Bera R, Hassan A, Goswami S, Das N (2020) Synthesis, characterization and adsorption studies of a novel triptycene based hydroxyl azo- nanoporous polymer for environmental remediation. *J Environ Chem Eng* 8:103558. <https://doi.org/10.1016/j.jece.2019.103558>
- Chairunnisa MF, Miyazaki T, Thu K, Miyawaki J, Nakabayashi K, Wijayanta AT, Rahmawati F (2020) Enhancing water adsorption capacity of acorn nutshell based activated carbon for adsorption thermal energy storage application. *Energy Rep* 6:255–263. <https://doi.org/10.1016/j.egy.2020.11.038>
- Freundlich HMF (1906) Over the adsorption in solution. *J Phys Chem* 57:385–470
- Fu JW, Chen ZH, Wu XC, Wang MH, Wang XZ, Zhang JH, Zhang JN, Xu Q (2015) Hollow poly(cyclotriphosphazene-co-phloroglucinol) microspheres: an effective and selective adsorbent for the removal of cationic dyes from aqueous solution. *Chem Eng J* 281:42–52. <https://doi.org/10.1016/j.cej.2015.06.088>
- Gao T, Yu J, Zhou Y, Jiang X (2017) The synthesis of graphene oxide functionalized with dithiocarbamate group and its prominent performance on adsorption of lead ions. *J Taiwan Inst Chem Eng* 71:426–432. <https://doi.org/10.1016/j.jtice.2016.11.033>
- Ho YS, McKay G (1999) Pseudo-second order model for sorption processes. *Process Biochem* 34:451–465. [https://doi.org/10.1016/S0032-9592\(98\)00112-5](https://doi.org/10.1016/S0032-9592(98)00112-5)
- Huang J, Wang X, Huang K (2009) Adsorption of *p*-nitroaniline by phenolic hydroxyl groups modified hyper-cross-linked polymeric adsorbent and XAD-4: a comparative study. *Chem Eng J* 155:722–727. <https://doi.org/10.1016/j.cej.2009.09.012>
- Huo J, Luo B, Chen Y (2019) Crystalline covalent organic frameworks from triazine nodes as porous adsorbents for dye pollutants. *ACS Omega* 4:22504–22513. <https://doi.org/10.1021/acsomega.9b03176>



- Jayasanthi Kumari H, Krishnamoorthy P, Arumugam TK, Radhakrishnan S, Vasudevan D (2017) An efficient removal of crystal violet dye from waste water by adsorption onto TLAC/Chitosan composite: a novel low cost adsorbent. *Int J Biol Macromol* 96:324–333. <https://doi.org/10.1016/j.ijbiomac.2016.11.077>
- Kim MM, Kim SK (2010) Effect of phloroglucinol on oxidative stress and inflammation. *Food Chem Toxicol* 48:2925–2933. <https://doi.org/10.1016/j.fct.2010.07.029>
- Langmuir I (1916) The constitution and fundamental properties of solids and liquids. Part I. solids. *J Am Chem Soc* 38:2221–2295. <https://doi.org/10.1021/ja02268a002>
- Li B, Guo JZ, Lv KL, Fan JJ (2019) Adsorption of methylene blue and Cd(II) onto maleylated modified hydrochar from water. *Environ Pollut* 254:113014. <https://doi.org/10.1016/j.envpol.2019.113014>
- Li B, Guo JZ, Liu JL, Fang L, Lv JQ, Lv K (2020) Removal of aqueous-phase lead ions by dithiocarbamate-modified hydrochar. *Sci Total Environ* 714:136897. <https://doi.org/10.1016/j.scitotenv.2020.136897>
- Li F, Zimmerman AR, Hu X, Yu Z, Huang J, Gao B (2020) One-pot synthesis and characterization of engineered hydrochar by hydrothermal carbonization of biomass with ZnCl₂. *Chemosphere* 254:126866. <https://doi.org/10.1016/j.chemosphere.2020.126866>
- Li HZ, Zhang YN, Guo JZ, Lv JQ, Huan WW, Li B (2021) Preparation of hydrochar with high adsorption performance for methylene blue by co-hydrothermal carbonization of polyvinyl chloride and bamboo. *Bioresour Technol* 337:125442. <https://doi.org/10.1016/j.biortech.2021.125442>
- Li Z, Xiao D, Ge Y, Koehler S (2015) Surface-functionalized porous lignin for fast and efficient lead removal from aqueous solution. *ACS Appl Mater Interfaces* 7:15000–15009. <https://doi.org/10.1021/acsami.5b03994>
- Lian QY, Yao LG, Ahmad ZU, Gang DD, Konggidinata I, Gallo AA, Zappi ME (2020) Enhanced Pb(II) adsorption onto functionalized ordered mesoporous carbon (OMC) from aqueous solutions: the important role of surface property and adsorption mechanism. *Environ Sci Pollut Res* 27:23616–23630. <https://doi.org/10.1007/s11356-020-08487-9>
- Lima EC, Hosseini-Bandegharai A, Moreno-Piraján JC, Anastopoulos I (2019) A critical review of the estimation of the thermodynamic parameters on adsorption equilibria. Wrong use of equilibrium constant in the Van't Hoff equation for calculation of thermodynamic parameters of adsorption. *J Mol Liq* 273:425–434. <https://doi.org/10.1016/j.molliq.2018.10.048>
- Liu B, Liu J, Huang D, Wei J, Di D (2020) Boric acid modified macroporous adsorption resin and its adsorption properties for catechol compounds. *Colloids Surf A: Physicochem Eng Aspects* 595:124674. <https://doi.org/10.1016/j.colsurfa.2020.124674>
- Lu S, Liu Q, Han R, Guo M, Shi J, Song C, Ji N, Lu X, Ma D (2021) Potential applications of porous organic polymers as adsorbent for the adsorption of volatile organic compounds. *J Environ Sci* 105:184–203. <https://doi.org/10.1016/j.jes.2021.01.007>
- Lv BW, Xu H, Guo JZ, Bai LQ, Li B (2022) Efficient adsorption of methylene blue on carboxylate-rich hydrochar prepared by one-step hydrothermal carbonization of bamboo and acrylic acid with ammonium persulphate. *J Hazard Mater* 421:126741. <https://doi.org/10.1016/j.jhazmat.2021.126741>
- Madduri S, Elsayed I, Hassan EB (2020) Novel oxone treated hydrochar for the removal of Pb(II) and methylene blue (MB) dye from aqueous solutions. *Chemosphere* 260:127683. <https://doi.org/10.1016/j.chemosphere.2020.127683>
- Mansha M, Waheed A, Ahmad T, Kazi IW, Ullah N (2020) Synthesis of a novel polysuccinimide based resin for the ultrahigh removal of anionic azo dyes from aqueous solution. *Environ Res* 184:109337. <https://doi.org/10.1016/j.envres.2020.109337>
- Muscarella SM, Badalucco L, Cano B, Laudicina VA, Mannina G (2021) Ammonium adsorption, desorption and recovery by acid and alkaline treated zeolite. *Bioresour Technol* 341:125812. <https://doi.org/10.1016/j.biortech.2021.125812>
- Pang J, Fu F, Ding Z, Lu J, Li N, Tang B (2017) Adsorption behaviors of methylene blue from aqueous solution on mesoporous birnessite. *J Taiwan Inst Chem Eng* 77:168–176. <https://doi.org/10.1016/j.jtice.2017.04.041>
- Peng H, Gao P, Chu G, Pan B, Peng J, Xing B (2017) Enhanced adsorption of Cu(II) and Cd(II) by phosphoric acid-modified biochars. *Environ Pollut* 229:846–853. <https://doi.org/10.1016/j.envpol.2017.07.004>
- Petrović JT, Stojanović MD, Milojković JV, Petrović MS, Šoštarić TD, Laušević MD, Mihajlović ML (2016) Alkali modified hydrochar of grape pomace as a perspective adsorbent of Pb²⁺ from aqueous solution. *J Environ Manage* 182:292–300. <https://doi.org/10.1016/j.jenvman.2016.07.081>
- Qian WC, Luo XP, Wang X, Guo M, Li B (2018) Removal of methylene blue from aqueous solution by modified bamboo hydrochar. *Ecotoxicol Environ Saf* 157:300–306. <https://doi.org/10.1016/j.ecoenv.2018.03.088>
- Salehi S, Alijani S, Anbia M (2020) Enhanced adsorption properties of zirconium modified chitosan-zeolite nanocomposites for vanadium ion removal. *Int J Biol Macromol* 164:105–120. <https://doi.org/10.1016/j.ijbiomac.2020.07.055>
- Sun S, Sha X, Liang J, Yang G, Hu X, Wen Y, Liu M, Zhou N, Zhang X, Wei Y (2021) Construction of ionic liquid functionalized MXene with extremely high adsorption capacity towards iodine via the combination of mussel-inspired chemistry and Michael addition reaction. *J Colloid Interface Sci* 601:294–304. <https://doi.org/10.1016/j.jcis.2021.05.096>
- Vinodha R, Gopi CVVM, Yang ZM, Deviprasath C, Atchudan R, Raman V, Yi M, Kim HJ (2020) Novel electrode material derived from porous polymeric organic framework of phloroglucinol and terephthaldehyde for symmetric supercapacitors. *J Energy Storage* 28:101283. <https://doi.org/10.1016/j.est.2020.101283>
- Wang Q, Zheng C, Shen Z, Lu Q, He C, Zhang TC, Liu J (2019) Polyethyleneimine and carbon disulfide co-modified alkaline lignin for removal of Pb²⁺ ions from water. *Chem Eng J* 359:265–274. <https://doi.org/10.1016/j.cej.2018.11.130>
- Wu Z, Zhong H, Yuan X, Wang H, Wang L, Chen X, Zeng G, Wu Y (2014) Adsorptive removal of methylene blue by rhamnolipid-functionalized graphene oxide from wastewater. *Water Res* 67:330–344. <https://doi.org/10.1016/j.watres.2014.09.026>
- Xia Y, Yang T, Zhu N, Li D, Chen Z, Lang Q, Liu Z, Jiao W (2019) Enhanced adsorption of Pb(II) onto modified hydrochar: modeling and mechanism analysis. *Bioresour Technol* 288:121593. <https://doi.org/10.1016/j.biortech.2019.121593>
- Xue Y, Gao B, Yao Y, Inyang M, Zhang M, Zimmerman AR, Ro KS (2012) Hydrogen peroxide modification enhances the ability of biochar (hydrochar) produced from hydrothermal carbonization of peanut hull to remove aqueous heavy metals: batch and column tests. *Chem Eng J* 200–202:673–680. <https://doi.org/10.1016/j.cej.2012.06.116>



- Zheng LC, Peng D, Meng PP (2018) Promotion effects of nitrogenous and oxygenic functional groups on cadmium (II) removal by carboxylated corn stalk. *J Clean Prod* 201:609–623. <https://doi.org/10.1016/j.jclepro.2018.08.070>
- Zhou Y, Qin L, Wu MK, Han L (2018) A bifunctional anionic metal-organic framework: reversible photochromism and selective adsorption of methylene blue. *Cryst Growth Des* 18:5738–5744. <https://doi.org/10.1021/acs.cgd.8b00895>

Springer Nature or its licensor (e.g. a society or other partner) holds exclusive rights to this article under a publishing agreement with the author(s) or other rightsholder(s); author self-archiving of the accepted manuscript version of this article is solely governed by the terms of such publishing agreement and applicable law.

